Journal of Applied Polymer Science

Fabrication of PCL/β-TCP scaffolds by 3D mini-screw extrusion printing

J. L. Dávila,[1,2] M. S. Freitas,[2,3] P. Inforçatti Neto,[2] Z. C. Silveira,[3] J. V. L. Silva,[2] M. A. d'Ávila[1]
[1]Department of Manufacturing and Materials Engineering, Faculty of Mechanical Engineering, University of Campinas, Campinas, SP, Brazil
[2]3-D Technologies Division, Renato Archer Information Technology Center, Campinas, SP, Brazil
[3]Department of Mechanical Engineering, São Carlos School of Engineering, University of São Paulo, São Carlos, SP, Brazil
Correspondence to: J. L. Dávila (E-mail: josedavila@fem.unicamp.br) and M. A. d'Ávila (E-mail: madavila@fem.unicamp.br)

ABSTRACT: Scaffolds of polycaprolactone (PCL) and PCL composites reinforced with β-tricalcium phosphate (β-TCP) were manufactured aiming potential tissue engineering applications. They were fabricated using a three-dimensional (3D) mini-screw extrusion printing, a novel additive manufacturing process, which consists in an extrusion head coupled to a 3D printer based on the Fab@Home equipment. Thermal properties were obtained by differential scanning calorimetry and thermogravimetric analyses. Scaffolds morphology were observed using scanning electron microscopy and computed microtomography; also, reinforcement presence was observed by X-ray diffraction and the polymer chemical structure by Fourier transform infrared spectroscopy. Mechanical properties under compression were obtained by using a universal testing machine and hydrophilic properties were studied by measuring the contact angle of water drops. Finally, scaffolds with 55% of porosity and a pore size of 450 μm have shown promising mechanical properties; the β-TCP reinforcement improved mechanical and hydrophilic behavior in comparison with PCL scaffolds. © 2015 Wiley Periodicals, Inc. J. Appl. Polym. Sci. **2016**, *133*, 43031.

KEYWORDS: biomaterials; composites; manufacturing

Received 20 August 2015; accepted 4 October 2015
DOI: 10.1002/app.43031

INTRODUCTION

The main goal of tissue engineering is to develop biological substitutes to restore, maintain, or improve the functions of different kinds of normal and pathological mammalian tissues.[1,2] Scaffolds are biological substitutes that mimic the extracellular matrix (ECM); they are temporary structures that allow cell attachment and cell growth.[3–5] Tissue engineering is a viable solution to the limitations of conventional treatments, which are mainly restricted due to the small number of donors.[6] This is an interdisciplinary research field, where the principles of engineering and life sciences are combined to fabricate scaffolds.[2] In this context, additive manufacturing (AM) processes have gained attention since these processes allow the generation of scaffolds with controlled geometry and suitable properties for tissue engineering applications. Biocompatibility, bioactivity, bioresorption, mechanical strength, and porosity are the main requirements of scaffolds. These characteristics can be achieved using both, biomaterials and AM processes.[7,8]

There are different AM processes that can be used to fabricate scaffolds for tissue engineering applications. The most common are Stereolithography (SL), Selective Laser Sintering (SLS), three-dimensional (3D) printing (3DP), and Fused Deposition Modeling (FDM). These processes have been grouped according to the ASTM F2792-12a process categories; SL is a vat photopolymerization process, SLS is a powder bed fusion process, 3DP is a material jetting process and FDM is a material extrusion process.[9] Moreover, 3D mini-screw extrusion based on FDM technology used in this research presents three innovative characteristics for portable 3D printer: it allows the use of small amounts of raw powder material (30–60 g), it is possible to reuse powder from SLS technology and it allows a better processing control.[10] Conversely, in commercial printers the process is tightly connected with their own supplied materials, which may not be suitable for biomedical applications. On the other hand, running specific medical grade materials is not possible in commercial printers, since printer parameters are not opened and consequently the printer cannot be configured to process different types of materials. The great advantage of the screw head is the possibility to mix different materials to create composite scaffolds; for example, with a trade-off solution of degradation rate and stiffness. In the 3D mini-screw system, a wide range of operating parameters is available, where the screw works with a maximum torque of 26 Nm, which allows

processing polymeric materials and polymer matrix composites. A maximum head speed of 12 mm/s for depositing the material and screw rotations in the range of 3–12.5 rpm can be readily set for scaffolds fabrication.

Polycaprolactone (PCL) is an aliphatic polyester biodegradable, bioresorbable, and biocompatible commonly used as biomaterial.[11] It has been widely used for bone and cartilage potential applications due to its mechanical properties.[12,13] However, its hydrophobicity can affect cell adhesion and proliferation.[2,14,15] Therefore, PCL composites and polymer blends have been fabricated to improve the scaffolds performance. Bioceramics such as hydroxyapatite (HA) and tricalcium phosphates (TCP) have been used as reinforcement of polymer matrix composites. These bioceramics are bioactive materials, which have appropriate biological properties in order to promote osteointegration.[16–18] In addition, 3D mini-screw extrusion printing allows fabricating PCL scaffolds and composite scaffolds, starting from polymer and ceramic powders without requiring the fabrication of filaments or pellets as in other extrusion processes.[10]

In this research, PCL and PCL/β-TCP scaffolds were fabricated by 3D mini-screw extrusion printing. The β-TCP was used as reinforcement to enhance mechanical and hydrophilic properties. The influence of β-TCP in the polymer matrix was studied; morphological, thermal, mechanical, and chemical properties were analyzed. Furthermore, β-TCP reinforcement was used because it shows higher bioresorption than α-TCP and HA.[17] The aim of this work was to fabricate scaffolds with 0°/90° architecture, from raw materials in powder form. To achieve good morphologies, a path generator software was developed. This program is compatible with the Fab@Home software and allows generating continuous 0°/90° 3D paths to print scaffolds.

EXPERIMENTAL

Materials

PCL CAPA® 6505 ($M_w = 50{,}000$ g/mol) was purchased from Rhodia Solvay Group. This polymer is in powder form; 97.5% of the material has a particle size less than 500 μm. Melting point is in the range of 58°C to 60°C. The bioceramic powder (β-TCP) was provided by the Ceramics Laboratory of LABIOMEC—UNICAMP with a mean particle size of 8 μm and particles in the range of 0.05–50 μm.

METHODS

Scaffold Fabrication

PCL and PCL/β-TCP scaffolds were fabricated with 0°/90° architecture. They were identified by the weight content of polymer and ceramic as follows: P100C0 for PCL pure scaffolds, P90C10, P80C20, and P70C30 for composite scaffolds. The powders were weighed on analytical balance and mixed in a mortar. All scaffolds were fabricated at 105°C. Extruder head speeds of 11.5 and 12 mm/s were fixed for PCL and PCL/β-TCP scaffolds, respectively. Screw rotation of 7.5 rpm was defined for all scaffold groups. Essentially, the used equipment is an interchangeable head that works coupled with the Fab@CTI 3D printer, as showed in Figure 1. In addition, a nozzle of 400 μm in diameter was used. To generate the 3D printing path, software named BioScaffolds PG was developed using Visual Basic. This software generates a 0°/90° vector with a continuous path, where the user can easily define the scaffold geometrical parameters. Then, a *.txt file compatible with the Fab@Home software is created. The continuous path is an advantage since the 3D printer does not need to stop the process between layers, minimizing morphological defects due to the additive process.

Morphological Characterization

In order to analyze scaffolds morphology, a Zeiss Evo MA 15 Scanning Electron Microscope (SEM) was used. Surface and cross section were observed. Specimens were fractured using liquid nitrogen and coated with a conductive layer of sputtered gold in a Bal-Tec SCD 050 Sputter Coater. Measurement of extruded strands diameter and pore size was performed using ImageJ 1.47v. Mean diameters were determined by performing 100 random measurements. Scaffolds porosity was obtained by μ-CT analysis using a X-ray Skyscan 1074 μ-CT scanner at a voltage of 40 kV and a current of 1000 μA, The exposure time was 600 ms for all specimens; 400 scans were done with a step of 0.9° for a 360° reconstruction. The image capture software was Skycan 1074 v2.1. Porosity analyses were performed using CT v1.9.1.0 Analyser and 3D reconstructions were carried out using InVesalius 3.0. Specimens of approximately 10 × 10 × 2 mm were used for morphological characterizations.

Thermal Characterization

Differential scanning calorimetry (DSC) analyses were performed using the equipment DSC 200 F3 Maia—Netzsch. First heating was carried out between 20°C and 200°C. Then, specimens were cooled to −100°C and maintained at this temperature for 2 min. Finally, a second heating was performed up to 200°C. Heating and cooling rates were 10°C/min. All analyses were performed in a nitrogen atmosphere (50 mL/min). The data analysis was performed using Netzsch Thermal Analyses 6.0.0 Proteus; transition temperatures and enthalpies of fusion and crystallization were obtained in accordance with ASTM D3418-12.[19] Furthermore, thermogravimetric analyses (TGA) were performed using a Mettler Toledo TGA equipment. Heating rate of 10°C/min in the range from 25°C to 700°C was used. Analyses were performed in a nitrogen atmosphere (50 mL/min). Thermal characterization specimens of approximately 10 mg were used.

X-ray Diffraction (XRD)

XRD analyses were carried out in an X'Pert PRO PANalitycal diffractometer (PW3040/60), using a voltage of 40 kV and a current of 20 mA with a Cu-Kα tube with λ= 1.5405 Å. All analyses were carried out in the range of $20° \leq 2\theta \leq 40°$. With this analysis, the presence of β-TCP in the PCL matrix was evaluated. Raw materials were analyzed in powder form and composites using scaffolds with dimensions of 18 × 18 × 2 mm.

Fourier Transform Infrared Spectroscopy (FTIR)

The FTIR analyses were performed in a Bruker Tensor 27 spectrometer in order to determine structural changes in both PCL and PCL/β-TCP scaffolds. The transmittance was evaluated in the wave number range from 4000 to 600 cm^{-1}. Attenuated total reflection (ATR) mode was used with 32 scans for each specimen.

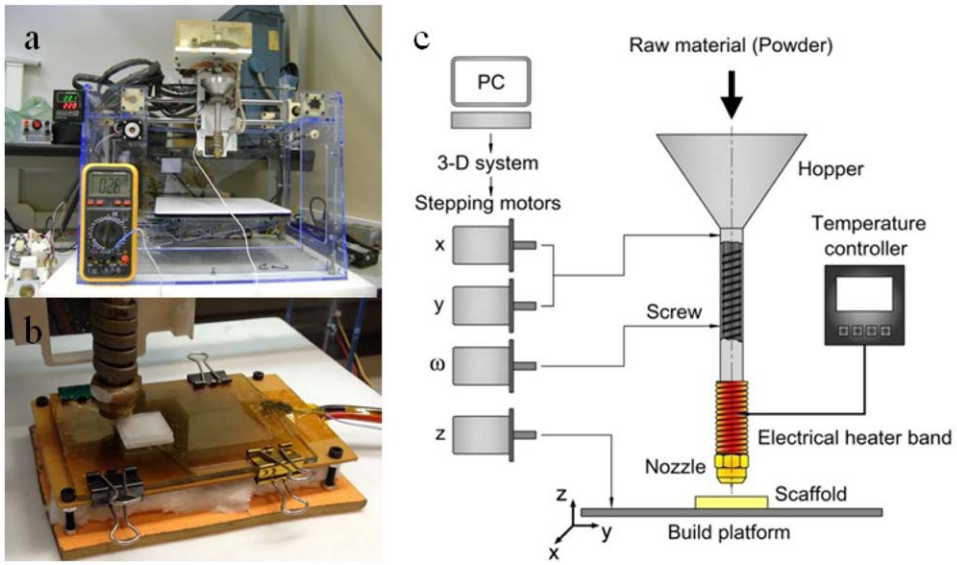

Figure 1. Fab@CTI 3D printer (interchangeable head): (a) Mini-screw head mounted on Fab@CTI platform, (b) scaffolds deposition using the mini-screw head, and (c) schematic illustration. [Color figure can be viewed in the online issue, which is available at wileyonlinelibrary.com.]

Mechanical Characterization

Mechanical properties were obtained by compression test. A universal testing machine MTS (Model 810-FlexTest 40) with a 1.5 kN load cell was used. Speed test was 1.3 mm/min. Five specimens with dimensions of 5 × 5 × 10 mm were tested for each scaffold group. The apparent compressive modulus was determined based on the slope of the linear region of the stress versus strain curve.

Water Contact Angle Measurement (WCA)

The water contact angle analyses were performed using a Hitachi microscope with AxioVision v4.8 software. For this test, non-porous specimens were fabricated with dimensions of 20 × 20 × 3 mm, in order to evaluate the hydrophilic properties of PCL and PCL/β-TCP surfaces. Deionized water drops of 5 μL were used. Drops were placed on the surfaces using a Transferpette pipette. All analyzes were performed with an environmental temperature of 26°C ± 2°C and a relative humidity of 46% ± 2%. For each group, five tests were carried out. An image was captured after place the drop and another after 300 s, in order to evaluate the variation of the angle over time. Contact angle measurements were performed using ImageJ 1.47v with Drop Analyses (ADSA-LB) plugin.

RESULTS AND DISCUSSION

Scaffold Fabrication and Morphology

Scaffolds were fabricated using BioScaffolds PG software to avoid stopping the process between layers. When the process stops, defects in the scaffold morphology can appear due to stress overshoot, material remains in the nozzle and the delayed response time[20]; this defects can be observed in the Figure 2(a,c). Conversely, continuous printing allowed fabricating scaffolds with better morphologies, as shown in Figure 2(b,d). On the other hand, Figure 3 shows SEM micrographs of 0°/90° architecture, strand surfaces and strand cross sections of the scaffolds. Microporosity in PCL scaffolds is observed in the Figure 3(a), which would be related to the screw extrusion process. These micropores make the surfaces of scaffold more roughened, which is a positive factor, since surface roughness can improve cell adhesion and proliferation.[8,21] With regard to composite scaffolds, Figure 3(b–d) show the presence of β-TCP particles in both, scaffold surfaces and cross section; in this case, microporosity did not appear due to β-TCP presence. As observed, β-TCP particles are dispersed in the polymer matrix. However, as shown in Figure 4, μ-CT analysis revealed a small amount of β-TCP agglomerations in the cross section of P80C20 scaffolds and a larger quantity in P70C30 scaffolds. All scaffold architectures presented good morphology and interconnected pores, as can be seen in Table I. Taking into account that scaffolds where fabricated with a 400-μm nozzle, strand diameter increased for all cases due to die swell, which is generated because of the elastic recovery when the strand leaves the

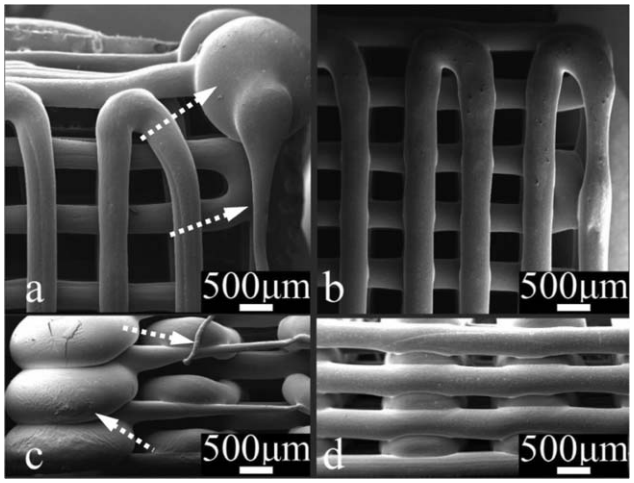

Figure 2. SEM micrographs of PCL scaffolds: (a,c) Morphological defects (*arrows* point to the defects locations) and (b,d) morphology without defects obtained by continuous additive process.

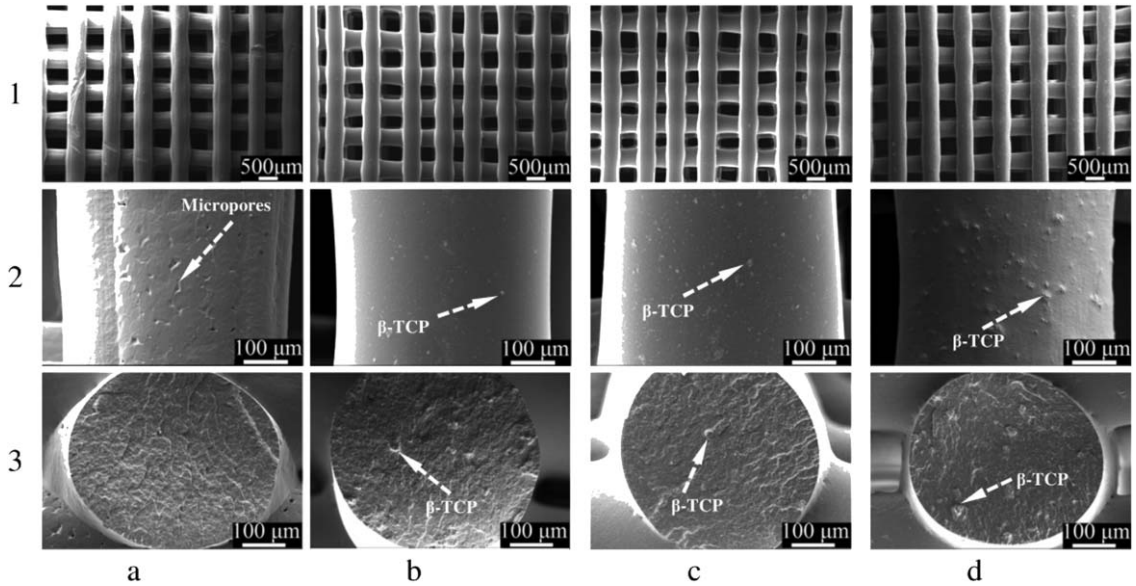

Figure 3. SEM micrographs of scaffolds: (a) P100C0, (b) P90C10, (c) P80C20, and (d) P70C30. (At row 1 is presented the 0°/90° architecture, at row 2 the strand surface and at row 3 the cross section of the strand).

nozzle.[16] Additionally, pore size and porosity were inside the adequate ranges commonly used for bone tissue applications. For bone tissue regeneration the minimum pore size recommended is 100 μm, but better osteogenesis is achieved with a pore size greater than 300 μm.[22] It was reported in the literature scaffolds with pore size up to 750 μm for bone tissue regeneration.[18] In relation to porosity, cortical bone is denser (porosity of 10% or less) than cancellous bone (porosity >50%).[23]

Thermal Properties and Composition

Second heating DSC curves of PCL CAPA® 6505, PCL scaffolds and composite scaffolds are showed in Figure 5(a). With these data, glass transition temperature (T_g), melting temperature (T_m), and melting enthalpy (ΔH_m) were obtained. Moreover, Figure 5(b) shows cooling DSC curves. With these data, crystallization enthalpy (ΔH_c) and crystallization temperature (T_c) were obtained. Crystallinity degree of PCL was determined using eq. (1),[24] where $\Delta H_m^0 = 139.5$ (J/g)[25,26] and ω is the polymer weight fraction.

$$\chi_c\,(\%) = \left(\frac{\Delta H_m}{\Delta H_m^0 \cdot \omega}\right) \times 100 \qquad (1)$$

Table II shows the results obtained by DSC analyses. T_g and T_m values did not show a significant variation and are around the theoretical values of PCL. Composites crystallization temperature T_c values were higher in comparison with PCL CAPA® 6505, which shows the influence of β-TCP as nucleating agent.[27] ΔH_m and ΔH_c values increased for PCL scaffolds in comparison with PCL CAPA® 6505 and decreased with the increment of β-TCP content; this behavior influenced the results obtained for crystallinity degree. Additionally, PCL scaffolds showed more crystallinity than PCL CAPA® 6505, which would be associated to heating during manufacturing process.[28,29] Crystallinity increased for composite scaffolds due to the nucleating effect of reinforcement.[27] As observed previously, μ-CT analyses revealed some agglomerations of β-TCP at higher concentrations; therefore, crystallinity degree would be affected by the presence of agglomerates.

TGA analyses were performed to determine the real composition of scaffolds. When TGA analyses of PCL are performed in nitrogen atmosphere, 5-hexanoic acid, CO_2, CO, and ε-caprolactone are liberated. In this case, thermal degradation curve shows one degradation stage; initially, 5-hexanoic acid and CO_2 are liberated. The peak degradation temperature for PCL was around 405°C for PCL and PCL/β-TCP scaffolds as observed in Figure 6(a). Above 430°C ε-caprolactone and CO vestiges are liberated.[30] On the other hand, β-TCP is stable up to 1125°C.[31] Therefore, as observed in Figure 6(b), within the temperature range fixed for the tests (25°C–700°C), PCL scaffolds showed practically complete mass loss. For composite

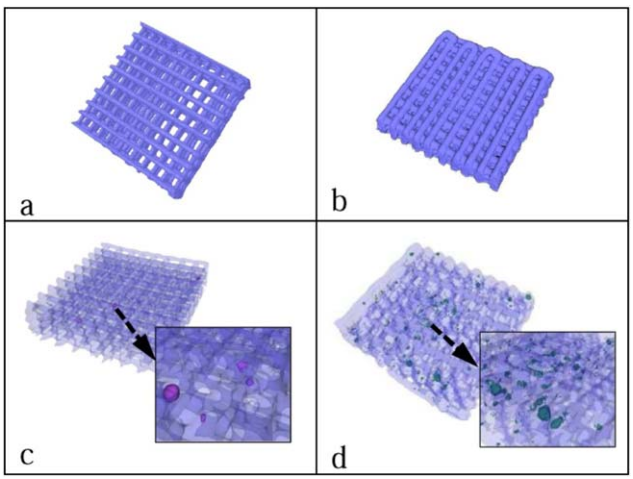

Figure 4. The 3D reconstructions generated from μ-CT data for scaffolds: (a) P100C0, (b) P90C10, (c) P80C20, and (d) P70C30. [Color figure can be viewed in the online issue, which is available at wileyonlinelibrary.com.]

Table I. Results of Morphological Characterization of PCL Scaffolds and PCL/β-TCP Composite Scaffolds

Sample	P100C0	P90C10	P80C20	P70C30
Strand diameter (μm)	453 ± 26	447 ± 14	453 ± 17	447 ± 24
Pore size (μm)	441 ± 59	430 ± 79	413 ± 104	447 ± 60
Porosity (%)	55.3 ± 0.5	57.2 ± 1.4	55.8 ± 1.1	55.7 ± 1.6

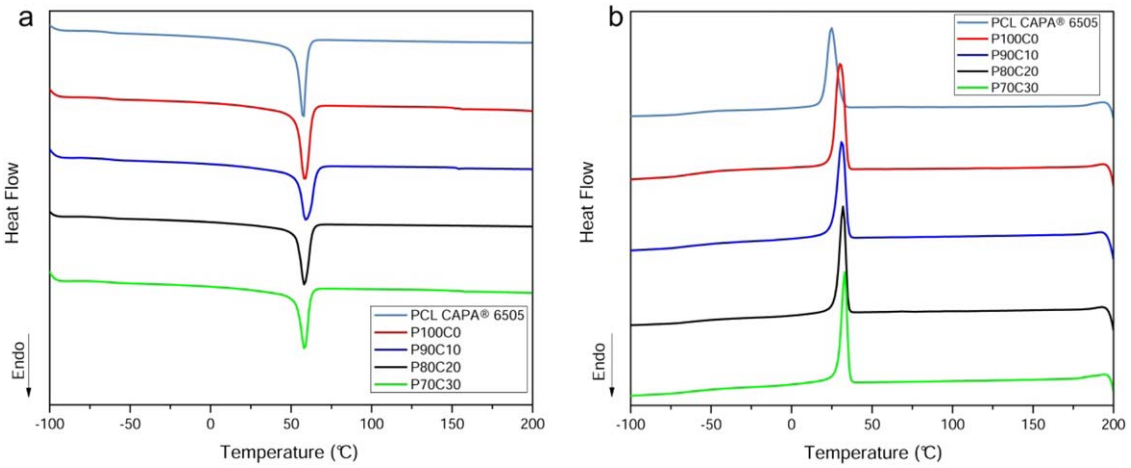

Figure 5. (a) Second heating DSC curves for PCL CAPA® 6505 and scaffolds. (b) DSC cooling curves for PCL CAPA® 6505 and scaffolds. [Color figure can be viewed in the online issue, which is available at wileyonlinelibrary.com.]

scaffolds it was possible to verify the real quantity of ceramic reinforcement, taking into account that β-TCP has no mass loss during the test.[16] Scaffolds P70C30 showed a larger divergence between real and theoretical compositions; it would be associated to the presence of reinforcement agglomerations. Additionally, XRD analyses showed scaffolds compositions qualitatively. PCL is a semicrystalline polymer; crystalline regions are constituted by orthorhombic unit cells.[17] The X-ray diffractometric pattern of PCL has basically three peaks associated to the planes (110), (111), and (200) around 2θ values of 21.4°, 21.9°, and 23.6°, respectively.[32,33] In Figure 7(a,b), the PCL and all the composite diffractometric patterns showed the three characteristic peaks. PCL CAPA® 6505 showed more intense peaks in comparison to the PCL and composite scaffolds. The porosity of scaffolds decreases the intensity of peaks. In contrast, the diffractometric pattern of β-TCP has some characteristic planes[34,35] as showed in Figure 7(b). Consequently, composite scaffolds revealed the influence of both, PCL and β-TCP. Composites with higher β-TCP content present peaks with higher intensity for β-TCP and less intensity for PCL, which is in agreement with TGA results.

Fourier Transform Infrared Spectroscopy (FTIR)

In Figure 8 it can be observed very similar FTIR spectra for all cases where the PCL is present, which means that polymer degradation during processing was not significant, mainly due to the fact that the band located at 1727 cm^{-1} is observed after processing, which is attributed to the carbonyl group (—C═O). Likewise, it is possible to observe two well-defined bands near 2949 cm^{-1} and 2865 cm^{-1}, which are associated with asymmetric and symmetric CH_2 stretching, respectively.[36] Additionally, the PCL peak temperature of thermal degradation is around 405°C, which suggests that no chemical transformations occurred during fabrication, since the system temperature was 105°C. On the other hand, the FTIR spectrum for β-TCP shows a band around 1020 cm^{-1}, which corresponds to calcium phosphate PO_4^{3-}.[37] In the FTIR spectra of composite scaffolds a strong influence of the β-TCP was not observed. For the three

Table II. Thermal Properties of PCL CAPA® 6505, PCL Scaffolds, and PCL/β-TCP Composite Scaffolds

Sample	T_g (°C)	T_m (°C)	T_c (°C)	ΔH_m (J/g)	ΔH_c (J/g)	χ_c (%)
PCL CAPA® 6505	−61.8	57.6	24.8	62.9	55.4	45.1
P100C0	−61.0	58.5	30.4	70.1	64.3	50.3
P90C10	−61.3	59.2	31.3	68.8	59.6	54.7
P80C20	−61.7	58.2	32.0	57.5	47.2	51.5
P70C30	−61.5	58.4	33.0	53.7	46.9	54.9

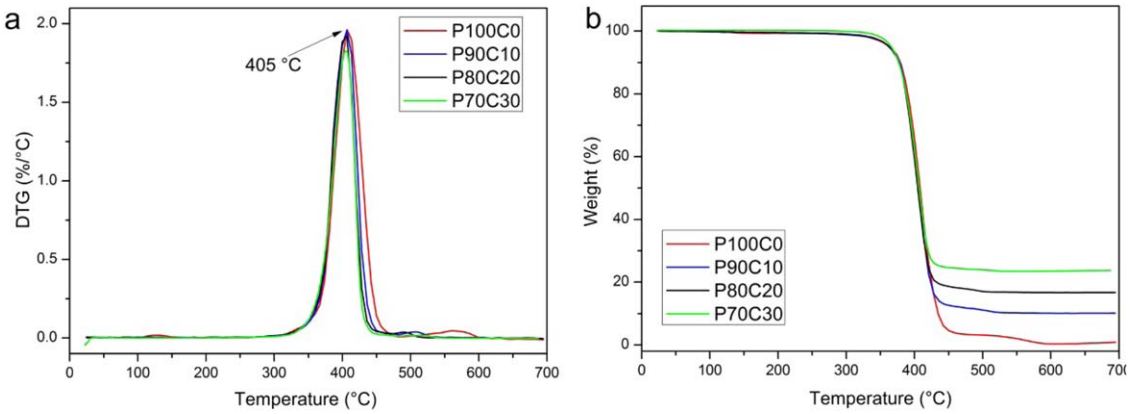

Figure 6. (a) TGA curves and (b) Derivative thermogravimetry (DTG) curves for PCL and PCL/β-TCP composite scaffolds. [Color figure can be viewed in the online issue, which is available at wileyonlinelibrary.com.]

compositions, the spectra were shifted slightly near the characteristic band of PO_4^{3-}. FTIR tests were conducted using the attenuated total reflection mode (ATR), that is, the sample analysis depth was typically in the range of micrometers, which would be associated to small influence of β-TCP in the FTIR spectra.

Mechanical Properties

One of a scaffold requirement is its compatibility with the mechanical properties of the host tissue. Scaffolds should provide a temporary support during the process of tissue regeneration.[7] That requirement was achieved with the four groups of scaffolds; Figure 9(a) shows stress versus strain curves and Figure 9(b) the apparent compressive modulus for PCL and composite scaffolds. P100C0, P90C10, and P80C20 scaffolds showed a mechanical behavior with a uniform trend within each group. Oppositely, P70C30 scaffolds showed a mechanical behavior with a greater variation. As observed in μ-CT analyses, scaffolds with a greater amount of reinforcement have higher agglomeration of β-TCP, which was related to the highest variation of mechanical properties. This agglomeration may be generated due to nozzle clogging[16] and the limited mixing capacity of the extruder screw. However, mechanical properties of all the scaffolds studied are within the range of applications in bone tissue, specifically cancellous bone; it has a compressive Young's modulus in the range of 20–500 MPa.[38,39] Bone is anisotropic and mechanical properties vary according to the bone localization in the body; that is, under compression, superior femoral bone has a strength of 2.35 MPa, inferior femoral bone 0.56 MPa, and proximal tibia 2.22 MPa.[40] Hence the fabricated scaffolds have good mechanical characteristics for applications in specific zones of the cancellous bone.

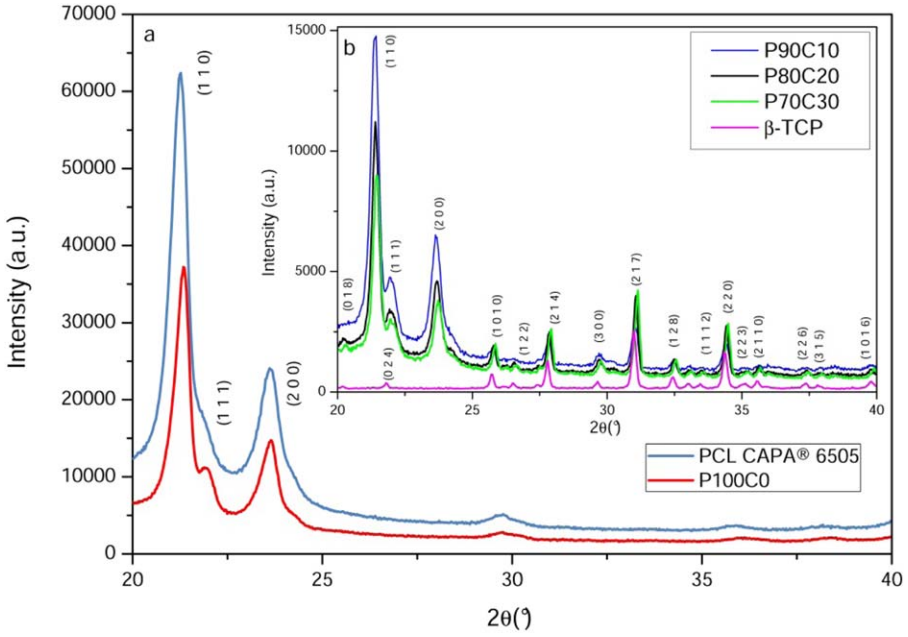

Figure 7. X-ray diffraction patterns: (a) PCL CAPA® 6505 and PCL scaffolds, (b) PCL/β-TCP composite scaffolds and β-TCP raw material. [Color figure can be viewed in the online issue, which is available at wileyonlinelibrary.com.]

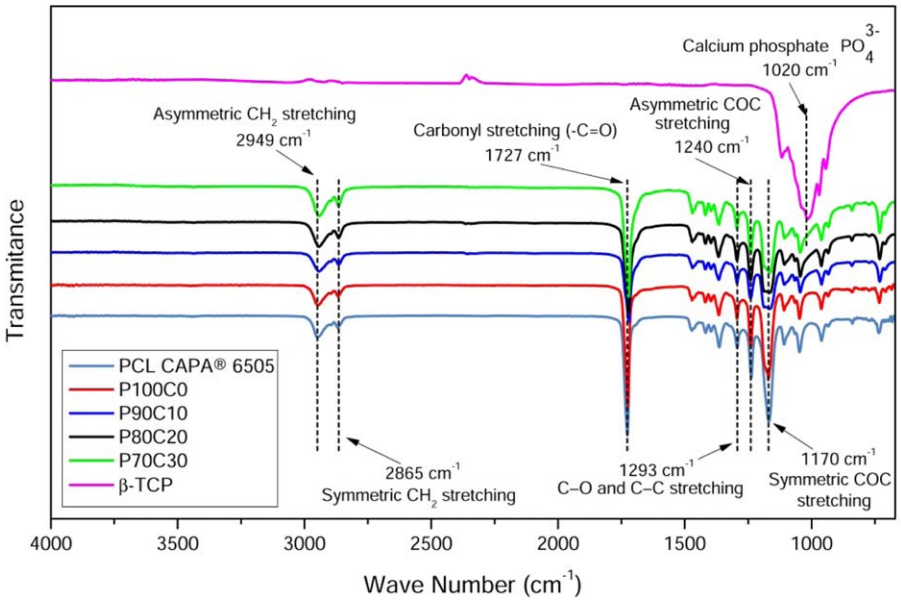

Figure 8. FTIR spectra for PCL CAPA® 6505, β-TCP, PCL scaffolds, and PCL/β-TCP composite scaffolds. [Color figure can be viewed in the online issue, which is available at wileyonlinelibrary.com.]

With more β-TCP content, the stiffness of scaffolds increased. For P90C10 scaffolds, the elastic modulus increased 26% compared with P100C0 scaffolds. In the case of P80C20 scaffolds, elastic modulus increased significantly, specifically 107% and P70C30 scaffolds showed an increase of 92%. The results show that the presence of β-TCP improved mechanical properties of the polymer matrix in all cases: the composition of 20% by weight has presented the best properties. Additionally, mechanical tests revealed that linear region is evident at low stress values, as reported in the literature.[12,28] Moreover, studies of mechanical behavior of scaffolds of PCL and PCL/HA show mechanical properties compatible with PCL and PCL/β-TCP scaffolds, in both cases suitable for bone tissue engineering applications. Scaffolds of PCL and PCL/HA obtained by precision extruding deposition have a compressive apparent modulus of 59 MPa and 84 MPa, respectively, and a porosity of 60% and 25% by weight content of HA.[18] Using β-TCP as reinforcement improved mechanical properties, taking into account that this allotropic form of TCP have reported better mechanical and biological properties than α-TCP and α'-TCP.[41] F-tests of equality of variances ($\alpha = 0.05$) between the analyzed groups confirmed significant difference between mechanical properties of the analyzed groups.

Hydrophilic Properties

Hydrophilic properties of biomaterials are of great importance in tissue engineering applications. Hydrophilicity of scaffold surfaces influences the behavior of cells, particularly in cell adhesion and proliferation. It also influences the adsorption of proteins, an important factor to start cell adhesion.[42,43] Figure 10 shows the results obtained for water contact angle measurements. As observed, the addition of the bioceramic improved

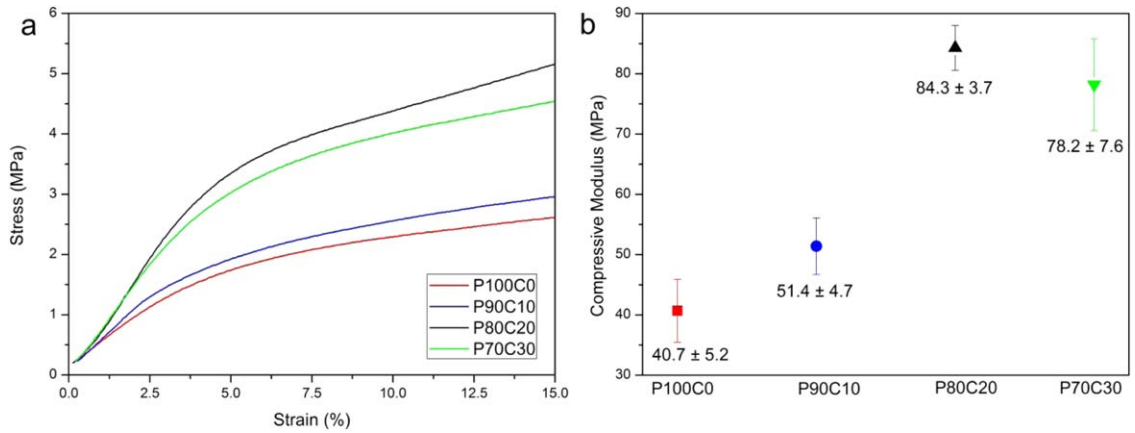

Figure 9. Mechanical properties: (a) Stress versus strain curves and (b) compressive modulus of PCL scaffolds and PCL/β-TCP composite scaffolds; mean and standard deviation. [Color figure can be viewed in the online issue, which is available at wileyonlinelibrary.com.]

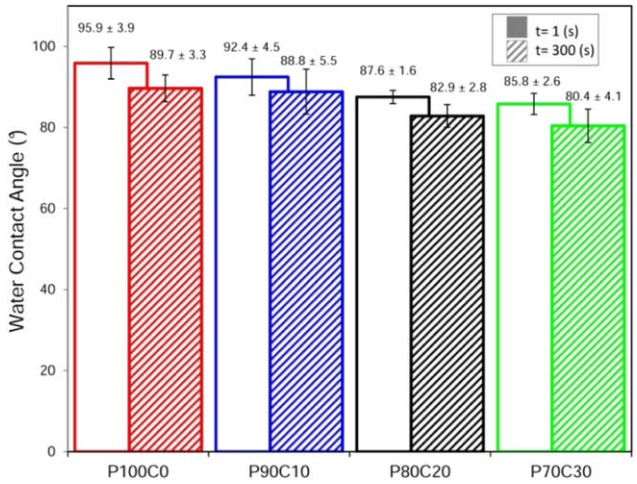

Figure 10. Water contact angle for PCL scaffolds and PCL/β-TCP composite scaffolds; mean and standard deviation. [Color figure can be viewed in the online issue, which is available at wileyonlinelibrary.com.]

hydrophilic properties. *F*-tests of equality of variances ($\alpha = 0.05$) and one-way analysis of variance ($\alpha = 0.05$) showed a significant difference between analyzed groups. According to literature, using bioceramics as reinforcement improves hydrophilic properties.[17,41,44] In this study, β-TCP slightly improved hydrophilic properties; when β-TCP content increases, water contact angle decreases.

CONCLUSIONS

PCL and PCL/β-TCP scaffolds were obtained by 3D mini-screw extrusion printing using the Fab@CTI 3D printer. The thermal characterization revealed that the reinforcement acted as nucleating agent, which allowed a better organization of polymer chains, increasing the crystallinity of polymer matrix. In addition, TGA allowed obtaining the real content of reinforcement in composite scaffolds. XRD analysis showed qualitatively the presence of β-TCP in the polymer matrix. Although some agglomerations of β-TCP were observed by μ-CT, all mechanical properties of composites were improved in comparison with PCL scaffolds; the composition of 20% by weight showed the best mechanical properties, but all groups of scaffolds have suitable mechanical properties for bone tissue applications. FTIR analyses showed the characteristic bands of the PCL structure, which suggest that the extrusion process did not change significantly the chemical structure of PCL. In PCL/β-TCP composites, hydrophilic properties improved slightly. Good morphology and properties were obtained; the fabricated scaffolds have potential for bone tissue applications. Future works will include *in vitro* tests.

ACKNOWLEDGMENTS

The authors acknowledge Secretaría de Educación Superior, Ciencia, Tecnología e Innovación (SENESCYT), Instituto Nacional de Ciência e Tecnologia em Biofabricação (INCT-BIOFABRIS), Centro de Tecnologia da Informação Renato Archer (CTI), Laboratório de Química do Estado Sólido (LQES-UNICAMP) for making available the use of the computed microtomography equipment and Conselho Nacional de Desenvolvimento Científico e Tecnológico (CNPq), Proc. 306860/2012-0 for financial support. J.L. Dávila thanks the MSc fellowship N° 251-2012 from SENESCYT.

REFERENCES

1. McIntire, L. V. WTEC Panel Report on Tissue Engineering Research; Academic Press: New York, **2003**.
2. Seyednejad, H.; Gawlitta, D.; Dhert, W. J. A.; van Nostrum, C. F.; Vermonden, T.; Hennink, W. E. *Acta Biomater.* **2011**, *7*, 1999.
3. Hutmacher, D. W. *J. Biomater. Sci. Polym. Ed.* **2001**, *12*, 107.
4. Yeong, W. Y.; Chua, C. K.; Leong, K. F.; Chandrasekaran, M. *Trends Biotechnol.* **2004**, *22*, 643.
5. Wang, M.; Ma, L.; Li, D.; Gao, C. *Polymer* **2013**, *54*, 277.
6. Yang, S.; Leong, K. F.; Du, Z.; Chua, C. K. *Tissue Eng.* **2002**, *8*, 1.
7. Bartolo, P.; Kruth, J. P.; Silva, J.; Levy, G.; Malshe, A.; Rajurkar, K.; Mitsuishi, M.; Ciurana, J.; Leu, M. *CIRP Ann. - Manuf. Technol.* **2012**, *61*, 635.
8. Sobral, J. M.; Caridade, S. G.; Sousa, R. A.; Mano, J. F.; Reis, R. L. *Acta Biomater.* **2011**, *7*, 1009.
9. Monzón, M. D.; Ortega, Z.; Martínez, A.; Ortega, F. *Int. J. Adv. Manuf. Technol.* **2015**, *76*, 1111.
10. Silveira, Z. C.; Freitas, M. S.; Inforçatti Neto, P.; Noritomi, P. Y.; Silva, J. V. L. *Key Eng. Mater.* **2014**, *572*, 151.
11. Cao, T.; Ho, K. H.; Teoh, S. H. *Tissue Eng.* **2003**, *9*, 103.
12. Kyriakidou, K.; Lucarini, G.; Zizzi, A.; Salvolini, E.; Belmonte, M. M.; Mollica, F.; Gloria, A.; Ambrosio, L. *J. Bioact. Compat. Polym.* **2008**, *23*, 227.
13. Williams, J. M.; Adewunmi, A.; Schek, R. M.; Flanagan, C. L.; Krebsbach, P. H.; Feinberg, S. E.; Hollister, S. J.; Das, S. *Biomaterials* **2005**, *26*, 4817.
14. Rodriguez, G.; Dias, J.; d'Ávila, M. A.; Bartolo, P. *Procedia Eng.* **2013**, *59*, 263.
15. Melchels, F. P. W.; Barradas, A. M. C.; Van Blitterswijk, C. A.; De Boer, J.; Feijen, J.; Grijpma, D. W. *Acta Biomater.* **2010**, *6*, 4208.
16. Yeo, M.; Jung, W. K.; Kim, G. *J. Mater. Chem.* **2012**, *22*, 3568.
17. Yeo, M.; Lee, H.; Kim, G. *Biomacromolecules* **2010**, *12*, 502.
18. Shor, L.; Yildirim, E. D.; Güçeri, S.; Sun, W. In Printed Biomaterials; Narayan, R.; Boland, T.; Lee, Y. S., Eds.; Springer: New York, **2010**, Chapter 2, p 91.
19. Vasquez, G. M.; Majewski, C. E.; Haworth, B.; Hopkinson, N. *Addit. Manuf.* **2014**, *1*, 127.
20. Giannitelli, S. M.; Accoto, D.; Trombetta, M.; Rainer, A. *Acta Biomater.* **2014**, *10*, 580.
21. Marcotte, L.; Tabrizian, M. *IRBM* **2008**, *29*, 77.
22. Hannink, G.; Arts, J. J. C. *Injury* **2011**, *42*, S22.
23. Bose, S.; Vahabzadeh, S.; Bandyopadhyay, A. *Mater. Today* **2013**, *16*, 496.

24. Lönnberg, H.; Fogelström, L.; Samir, M. A. S. A.; Berglund, L.; Malmström, E.; Hult, A. *Eur. Polym. J.* **2008**, *44*, 2991.
25. Guarino, V.; Lewandowska, M.; Bil, M.; Polak, B.; Ambrosio, L. *Compos. Sci. Technol.* **2010**, *70*, 1826.
26. Gupta, B.; Ray, A. R. *J. Appl. Polym. Sci.* **2012**, *123*, 1944.
27. Patlolla, A.; Collins, G.; Arinzeh, T. L. *Acta Biomater.* **2010**, *6*, 90.
28. Zein, I.; Hutmacher, D. W.; Tan, K. C.; Teoh, S. H. *Biomaterials* **2002**, *23*, 1169.
29. Hutmacher, D. W.; Schantz, T.; Zein, I.; Ng, K. W.; Teoh, S. H.; Tan, K. C. *J. Biomed. Mater. Res.* **2001**, *55*, 203.
30. Vogel, C.; Siesler, H. W. *Macromol. Symp.* **2008**, *265*, 183.
31. Kwon, S. H.; Jun, Y. K.; Hong, S. H.; Kim, H. E. *J. Eur. Ceram. Soc.* **2003**, *23*, 1039.
32. Monteiro, M. S. S. B.; Chávez, F. V.; Sebastião, P. J.; Tavares, M. I. B. *Polym. Test.* **2013**, *32*, 553.
33. Xing, Z.; Yang, G. *J. Appl. Polym. Sci.* **2010**, *115*, 2747.
34. Sakka, S.; Ayed, F. B.; Bouaziz, J. In Advances in Biomaterials Science and Biomedical Applications; Pignatello, R. Ed.; INTECH Open Access Publisher: Croatia, **2013**, Chapter 2, p 23.
35. Tavares, D.; Castro, L.; Soares, G.; Alves, G.; Granjeiro, J. *J. Appl. Oral Sci.* **2013**, *21*, 37.
36. Elzein, T.; Nasser-Eddine, M.; Delaite, C.; Bistac, S.; Dumas, P. *J. Colloid Interface Sci.* **2004**, *273*, 381.
37. Bianco, A.; Di Federico, E.; Cacciotti, I. *Polym. Adv. Technol.* **2011**, *22*, 1832.
38. Goonoo, N.; Bhaw-Luximon, A.; Bowlin, G. L.; Jhurry, D. *Polym. Int.* **2013**, *62*, 523.
39. Yang, S.; Leong, K. F.; Du, Z.; Chua, C. K. *Tissue Eng.* **2001**, *7*, 679.
40. Cullinane, D. M.; Salisbury, K. T. In Bone Tissue Engineering; Hollinger, J. O.; Einhorn, T. A.; Doll, B.; Sfeir, C., Eds.; CRC Press: Boca Raton, **2004**; Chapter 10, p 245.
41. Wu, F.; Liu, C.; O'Neill, B.; Wei, J.; Ngothai, Y. *Appl. Surf. Sci.* **2012**, *258*, 7589.
42. Wei, J.; Igarashi, T.; Okumori, N.; Igarashi, T.; Maetani, T.; Liu, B.; Yoshinari, M. *Biomed. Mater.* **2009**, *4*, 045002.
43. Zhou, Y.; Hutmacher, D. W.; Varawan, S. L.; Lim, T. M. *Polym. Int.* **2007**, *56*, 333.
44. Lam, C. X. F.; Teoh, S.; Hutmacher, H. D. W. *Polym. Int.* **2007**, *56*, 718.